Journal of Engineering Mathematics (2006) 54: 319–331
DOI 10.1007/s10665-006-9034-5

Dam-break flow for arbitrary slopes of the bottom

R. FERNANDEZ-FERIA
Universidad de Málaga, E.T.S. Ingenieros Industriales, 29013 Málaga, Spain (E-mail: ramon.fernandez@uma.es)

Received 24 May 2004; accepted in revised form 9 January 2006 / Published online: 26 April 2006

Abstract. The dam-break flow problem in the shallow-water approximation on an inclined bed for arbitrary slopes of the bottom is considered. An analytical solution for the spreading of the water fronts at the initial stages is given. A self-similar solution asymptotically valid at large time is also found. For intermediate times the problem is solved numerically by the method of characteristics.

Key words: dam-break problem, method of characteristics, similarity solution, sloping channel

1. Introduction

Dam-break flows, *i.e.*, the instantaneous release of a fluid behind a vertical wall, constitutes an important problem in civil and hydraulic engineering. The interest of studying this type of flow resides not only on its practical importance for modelling the effects of the rupture of a dam on its surrounding environment, but also has a fundamental interest in fluid mechanics. Thus, among the simpler and more important non-trivial solutions to the so-called shallow-water equations are the well-known self-similar solution for the dam-break flow on a horizontal plane, first given by Ritter [1], and its extension for the dam-break flow upon a wet horizontal plane [2, Chapter 10].

In this note, the one-dimensional dam-break flow problem on an inclined dry plane with constant slope is considered. As a fundamental difference with the horizontal case, one has now a finite mass of liquid, being thus more realistic for modelling the movement of a flood wave down a river following a sudden release of water from a ruptured dam. A similar problem was considered previously by Hunt [3], but in a very different approach. That author, who also considered the case of a wet channel, used the so-called kinematic-wave approximation that makes use of approximate relations between the flow rate and the flow depth based on empirical friction laws. Here we consider the ideal-flow shallow-water equations and obtain analytical expressions for the movement of both the upstream and downstream water fronts, valid for the initial stages after the release of the fluid. Analogous solutions for the drying and wetting fronts were obtained by Hunt [4] in the limit of small channel slope, whereas here we consider the general case of arbitrary slope. In addition, we also give a self-similar solution for the movement of the whole mass of water asymptotically valid at large time. One of the motivations for this work has been to provide analytical solutions to validate numerical studies based on the shallow-water equations for the flow upon non-horizontal beds. In particular, for numerical schemes involving the advance of water fronts on a dry, inclined surface.

2. Formulation of the problem

The one-dimensional shallow-water equations have recently been generalized by Keller [5] to arbitrary slopes of the bottom by just using a scaling method (see also the earlier work by

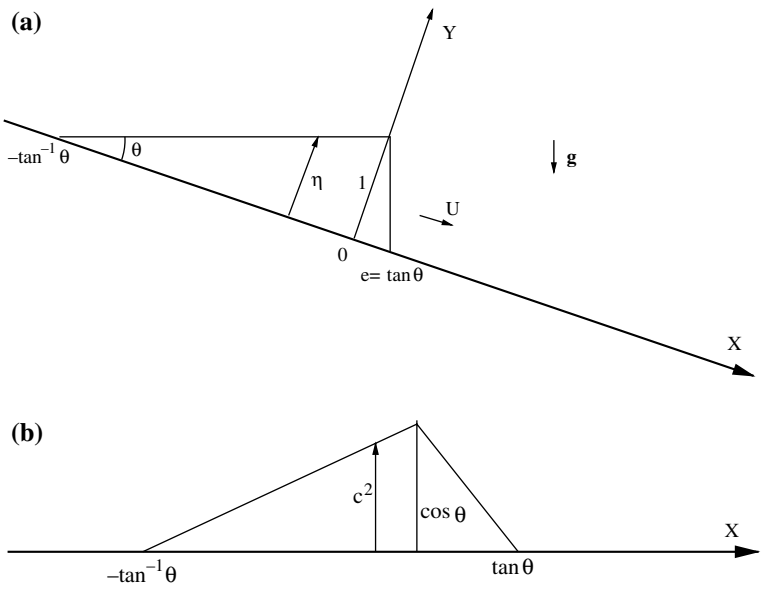

Figure 1. Coordinates and sketch of the initial conditions for $\eta(X)$ (a), and $c^2(x)$.

Savage and Hutter [6], and by Bouchut *et al.* [7]). These equations take a very simple form when the slope of the bed is *constant*, for $\theta_x = 0$, $J = 1$, and $h_t = 0$ in Equations (3.4–3.5) in [5] (note that there is a missprint in the sign of the last term of Equation (3.4) in [5]). Thus, the one-dimensional shallow-water equations for the flow over a constant (but arbitrary) sloping bed are formally the same as for a small bed angle (see, for example, [2, Chapter 2]), but with different notation [see Figure 1(a)]:

$$\frac{\partial \eta}{\partial t} + \frac{\partial \eta U}{\partial X} = 0, \tag{1}$$

$$\frac{\partial U}{\partial t} + U\frac{\partial U}{\partial X} + \cos\theta \frac{\partial \eta}{\partial X} = \sin\theta, \tag{2}$$

where θ is the angle between the bed and the horizontal (note that θ here is $-\theta$ in [5]), t is the time, X is the coordinate along the bed, η is the depth of the water measured along the coordinate Y perpendicular to the bed, and U is the depth-averaged velocity component along X [see Figure 1(a)]. All the magnitudes in the above equations are dimensionless, and have been non-dimensionalized with respect to a length scale η_0, corresponding to some initial depth, and a velocity scale $U_0 = \sqrt{g\eta_0}$, where g is the acceleration due to gravity.

We are interested here in solving these equations for the dam-break problem, *i.e.*, for the flow whose initial condition ($t = 0$) is given by [see Figure 1(a)]

$$U(0, X) = 0, \tag{3}$$

$$\eta(0, X) = \begin{cases} 0 & \text{for } X < -1/e \\ eX + 1 & \text{for } -1/e \le X \le 0 \\ -X/e + 1 & \text{for } 0 < X \le e \\ 0 & \text{for } X > e \end{cases}, \tag{4}$$

where

$$e \equiv \tan\theta \tag{5}$$

is the slope of the bed. At $t=0$, the vertical wall that intersects the bed at $X=e$ is removed instantaneously, causing the fluid to move over the sloping bed under the action of gravity. Note that characteristic length η_0 is the dimensional depth at $X=0$, $t=0$.

It is convenient to make the following change of variables,

$$x = X - \frac{1}{2}\sin\theta t^2, \quad u = U - \sin\theta t, \quad c = \sqrt{\eta\cos\theta}, \tag{6}$$

leaving t unchanged, which transforms Equations (1–2) and the initial condition (3–4) into (note that for $t=0$, $x=X$)

$$2\frac{\partial c}{\partial t} + c\frac{\partial u}{\partial x} + 2u\frac{\partial c}{\partial x} = 0, \tag{7}$$

$$\frac{\partial u}{\partial t} + u\frac{\partial u}{\partial x} + 2c\frac{\partial c}{\partial x} = 0, \tag{8}$$

$$u(0,x) = 0, \tag{9}$$

$$c(0,x) = \begin{cases} 0 & \text{for } x < -1/e \\ \sqrt{\cos\theta(1+ex)} & \text{for } -1/e \le x \le 0 \\ \sqrt{\cos\theta(1-x/e)} & \text{for } 0 < x \le e \\ 0 & \text{for } x > e \end{cases}. \tag{10}$$

Equations (7–8) are the shallow-water equations for the flow over a horizontal bed in terms of the non-dimensional horizontal velocity u and wave speed $c \equiv \sqrt{h}$, where h is the non-dimensional vertical depth. Therefore, with this change of variables, the original dam-break problem on a sloping bed is mathematically equivalent to the one-dimensional spreading of an initially triangle-shaped mass of water over a horizontal bed [see Figure 1(b)].

As it is well known, the characteristic form of equations (7–8) takes the very simple form (see, *e.g.*, [2, Chapter 10])

$$u + 2c = \text{constant} \quad \text{along} \quad \frac{\mathrm{d}x}{\mathrm{d}t} = u + c \quad (\text{characteristics } C_+), \tag{11}$$

$$u - 2c = \text{constant} \quad \text{along} \quad \frac{\mathrm{d}x}{\mathrm{d}t} = u - c \quad (\text{characteristics } C_-), \tag{12}$$

where $u \pm 2c$ are the Riemann invariants.

3. Analytic solution for the advance of the water-fronts at the initial stages

Equations (11–12) may be used to solve (7–8) numerically by the method of characteristics, starting from the initial conditions (9–10). However, at $t=0$, both fronts, at $x=-1/e$ and at $x=e$, where $c=u=0$, are singular points, so that the method of characteristics cannot be started from them. It would therefore be convenient to have a solution near these points at the initial stages after the dam-break. In addition to serve as the starting condition for the method of characteristics near these singular points, this solution will provide the spreading of the two water fronts at the initial stages after the collapse of the dam.

For sufficiently small t (see below), the solution near each of the two singular points $x=-1/e$ and $x=e$ depends only on the local values of c and u at the vicinity of them. Therefore, one may try to solve (7–8) with the initial condition $u(0,x)=0$, $c(0,x)=Ax^{1/2}$ for $x>0$,

and $c(0,x)=0$ for $x\le 0$, where A is any constant, which corresponds to an initial semi-infinite mass of water with linear depth to the right of $x=0$. This problem has the following exact analytical solution,

$$u(t,x)=-A^2t, \tag{13}$$

$$c(t,x)=\begin{cases} 0 & \text{for } x<-A^2t^2/2 \\ A\sqrt{x+A^2t^2/2} & \text{for } x\ge -A^2t^2/2 \end{cases}, \tag{14}$$

as may be checked by direct substitution in the equations and the fact that it satisfies the initial condition. Although not given explicitly, this solution is contained within the class of exact solutions to the shallow-water equations with linear velocity profiles given by [8]. The water front, initially at $x=0$, advances to the left according to the trajectory $x=l(t)\equiv -A^2t^2/2$. Although this might not be the only solution to the nonlinear problem, as commented on below it is the only physically relevant one for the particular cases of a horizontal, and a vertical, free surface on an inclined bed. Obviously, this solution is not valid for the classical dam-break problem on a horizontal plane [1], for which $A\to\infty$. The characteristics curves C_+ and C_- starting at $x_0>0$ for $t=0$ are

$$x=-\frac{A^2t^2}{4}+\sqrt{x_0}At+x_0 \quad (C_+), \tag{15}$$

$$x=-\frac{A^2t^2}{4}-\sqrt{x_0}At+x_0 \quad (C_-). \tag{16}$$

This solution is valid for sufficiently small t in the vicinity of both $x=-1/e$ and $x=e$ if one makes the changes of variables $x\mapsto x+1/e$, $A\mapsto\sqrt{\sin\theta}$, and $x\mapsto e-x$, $A\mapsto\sqrt{\cos\theta/e}$, respectively. That is to say, the initial stages of the advance of the left water front is given by

$$u(t,x)=-\sin\theta t, \tag{17}$$

$$c(t,x)=\begin{cases} 0 & \text{for } x<l_2^0(t)\equiv -1/e-\sin\theta t^2/2 \\ \sqrt{\sin\theta}\sqrt{x+1/e+\sin\theta t^2/2} & \text{for } x\ge -l_2^0(t) \end{cases}, \tag{18}$$

while that of the right front is given by

$$u(t,x)=\frac{\cos\theta}{e}t, \tag{19}$$

$$c(t,x)=\begin{cases} 0 & \text{for } x>l_1^0(t)\equiv e+\frac{\cos\theta}{e}\frac{t^2}{2} \\ \sqrt{\frac{\cos\theta}{e}}\sqrt{-x+e+\frac{\cos\theta}{e}\frac{t^2}{2}} & \text{for } x\le l_1^0(t) \end{cases}. \tag{20}$$

The validity range in the plane (x,t) of each one of these two solutions can be determined from the corresponding characteristics (15–16) starting at the point $x_0=0$. In view of Figure 2, the characteristic C_2, corresponding to the C_- characteristic obtained with (17–18) and starting at $(x_0=0,t=0)$, separates the region of influence of the right $(x>0)$ portion of the initial water depth $h(0,x)$ on the left portion of h ($h(0,x)$ is also plotted in Figure 2 for reference); *i.e.*, the solution (17–18) is valid to the left of $C_2(t)$. Thus, the advance of the left water front (17–18) is valid in the region of the (t,x) plane given by

$$l_2^0(t)=-\frac{1}{e}-\sin\theta\frac{t^2}{2}\le x\le C_2(t)=-\sqrt{\cos\theta}t-\sin\theta\frac{t^2}{4}. \tag{21}$$

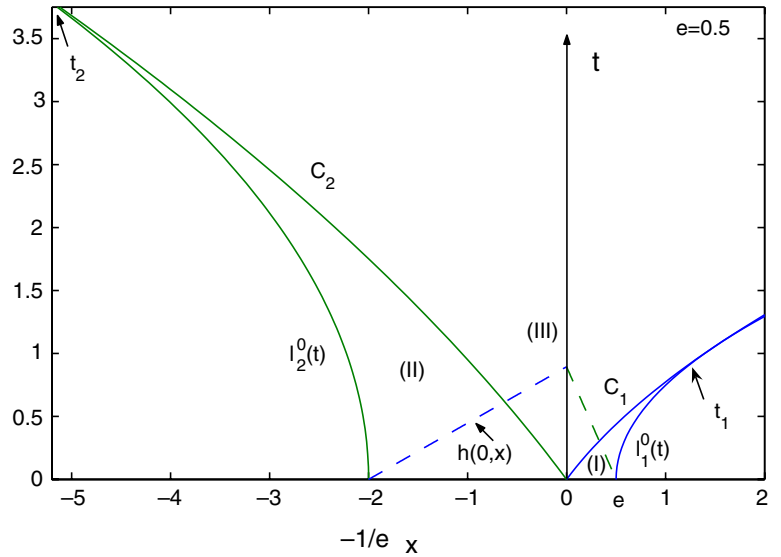

Figure 2. Water fronts at the initial stages, $l_1^0(t)$, $l_2^0(t)$, and characteristics $C_2(t)$ and $C_1(t)$ on the plane (x,t) for $e=0{\cdot}5$ ($t_2\simeq 4{\cdot}2$, $t_1\simeq 1{\cdot}1$). Also plotted for reference is the initial water-depth distribution $h(0,x)$.

This region is labelled with (II) in Figure 2. The curves $l_2^0(t)$ and $C_2(t)$ cross each other at the time

$$t_2 \equiv 2\frac{\sqrt{\cos\theta}}{\sin\theta}, \tag{22}$$

so that the solution is valid for $t \le t_2$. Note that t_2 may be very large if θ is small. Note also that during the interval of time for which this solution (17–18) is valid, in the original coordinate X on the inclined bed, both the left water front $L_2^0(t) \equiv l_2^0(t) + \frac{1}{2}\sin\theta t^2$ and the water level remain steady, $L_2^0 = -1/e$, and $\eta = e(X + 1/e)$, respectively, as it should be for a semi-infinite mass of water with a horizontal free surface.

Similarly, the solution (19–20) for the advance of the right water front is valid to the right of C_1, *i.e.*, in the region of the (t,x) plane given by

$$C_1(t) = \sqrt{\cos\theta}t + \frac{\cos\theta}{e}\frac{t^2}{4} \le x \le l_1^0(t) = e + \frac{\cos\theta}{e}\frac{t^2}{2}, \tag{23}$$

labelled with (I) in Figure 2. The curves $l_1^0(t)$ and $C_1(t)$ become tangent at

$$t_1 \equiv 2\frac{e}{\sqrt{\cos\theta}}. \tag{24}$$

Outside regions (I) and (II) [region (III) in Figure 2], the solution has to be obtained numerically (for instance by the method of characteristics; see next section), but these two solutions for the advances of the right (wetting) and left (drying) water fronts give analytically important information about the initial water spreading. The total extent of the water spreading is given by

$$l_s^0(t) \equiv l_1^0(t) - l_2^0(t) = e + \frac{1}{e} + \frac{1}{\sin\theta}\frac{t^2}{2}, \tag{25}$$

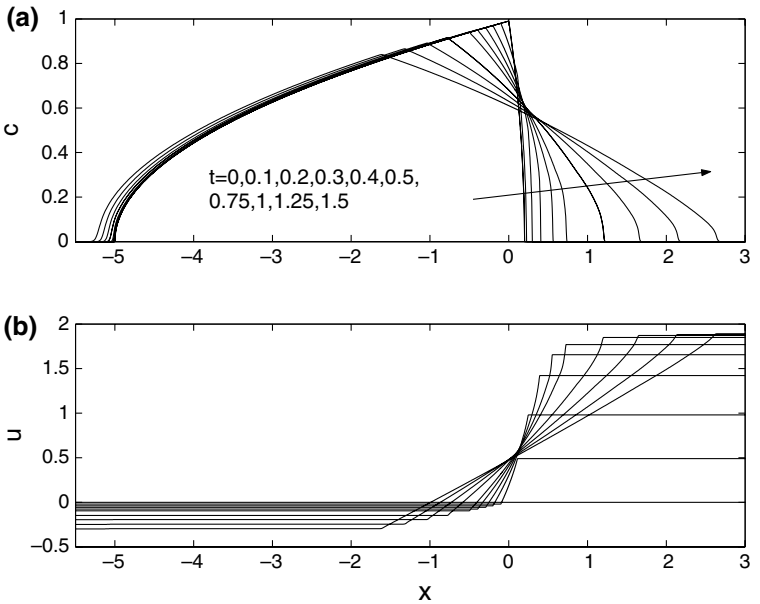

Figure 3. x-profiles of c (a) and u (b) for several instants of time, as indicated in (a), for $e=0{\cdot}2$.

valid for $t<t_i\equiv\min(t_1,t_2)$. In the original coordinate X along the inclined bed, the water extent for $t<t_i$ is [by using (6) and the expressions for l_1^0 and l_2^0]:

$$L_2^0(t)\equiv-\frac{1}{e}\le X\le L_1^0(t)\equiv e+\frac{1}{\sin\theta}\frac{t^2}{2}. \tag{26}$$

Note that the left water front remains at rest in the coordinate X for $t<t_2$, which is larger than t_1 if $\theta<45^o$ ($e<1$). Thus, the left (drying) water front remains at rest until the information about the break of the dam, travelling along the characteristic C_2, reaches it. This result coincides with that of [4] for small θ.

4. Numerical solution for $e=0{\cdot}2$

Figure 3 shows several x-profiles of c and u for different instants of time up to $t=1{\cdot}5$ when the slope is $e=0{\cdot}2$ ($\theta\simeq11{\cdot}31^o$). These solutions are obtained numerically by use of the method of characteristics based on (11–12), starting at $t=0$ with the initial distribution (9–10). A predictor-corrector method, second-order accurate in time, with a time step $\Delta t=0{\cdot}01$, is used. To avoid the singularity near the initial water fronts at $x=-1/e$ and $x=e$, the analytical solutions (17–18) and (19–20) are used, respectively, near these points for the first 20 time steps.

For this value of e, $t_1\simeq0{\cdot}4079$ and $t_2\simeq10{\cdot}0985$, so that the advance of the left front is given by $l_2^0(t)$ for all the values of t plotted in Figure 3, while the advance of the right front is given by $l_1^0(t)$ only for $0\le t\le t_1<1{\cdot}5$. This is illustrated in Figure 4, where the numerical values of the trajectories of the right and left fronts, $l_1(t)$ and $l_2(t)$, are compared to $l_1^0(t)$ and $l_2^0(t)$, respectively (note that a larger interval of time, $0\le t\le12$, is plotted in Figure 4(b)). Figure 5 shows the water-depth profiles, and the velocity U, in the original coordinate X along the sloping bed for the same instants of time as used in Figure 3. According to (6) and Figure 1, the horizontal and vertical coordinates in Figure 5(a) are, respectively,

$$\cos\theta\left(x+\frac{1}{2}\sin\theta t^2\right)+ec^2(t,x)\equiv x_e,\quad\text{and}\quad(1+e^2)c^2(t,x)-ex_e. \tag{27}$$

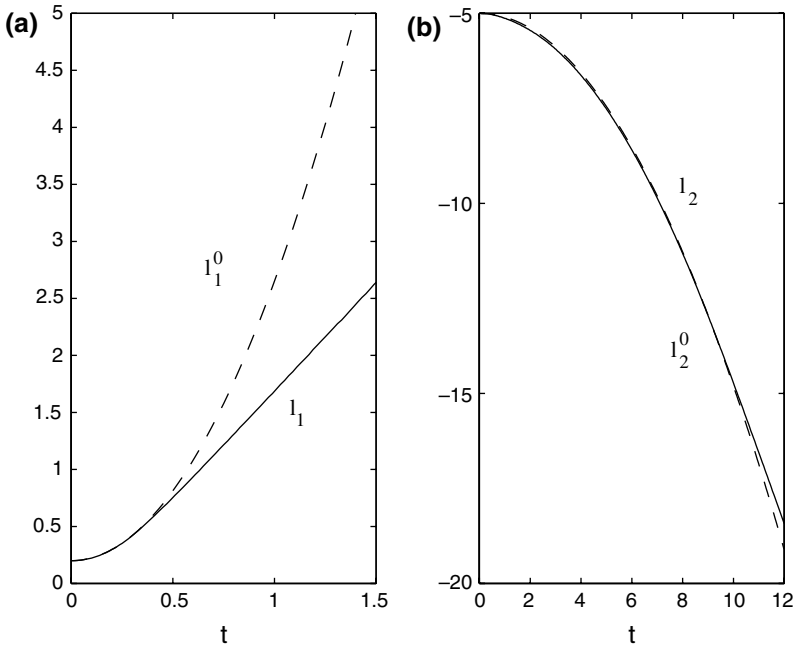

Figure 4. Right (a) and left (b) water fronts $l_1(t)$ and $l_2(t)$ obtained numerically (continuous lines) compared to $l_1^0(t)$ and $l_2^0(t)$ (dashed lines), for $e = 0{\cdot}2$. Both curves coincide for the right front up to $t = t_1 \simeq 0{\cdot}4039$, while for the left front (b) they are practically the same up to $t = t_2 \simeq 10{\cdot}0985$.

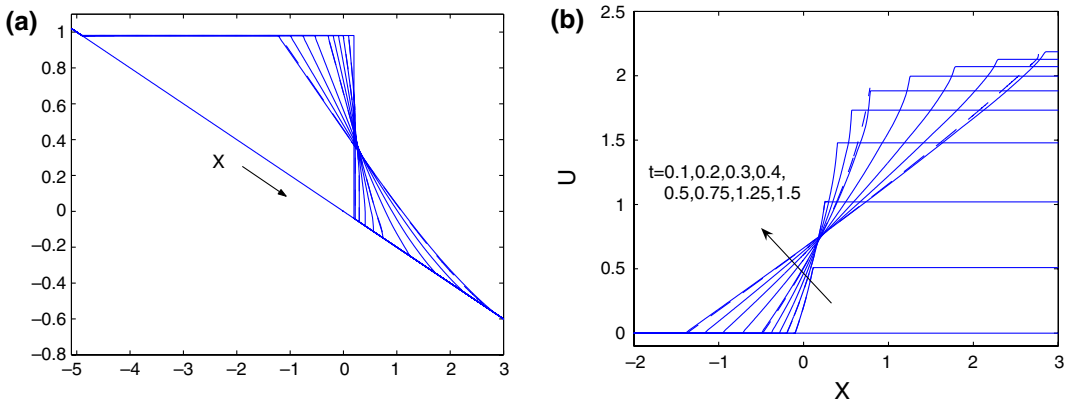

Figure 5. Water depths (a) and velocity U (b) in the original coordinate X along the sloping bed for $e = 0{\cdot}2$ and for the same instants of time depicted in Figure 3. Also plotted with dashed lines are the solutions obtained from a finite-volume method [9] at the instants $t = 0{\cdot}1, 0{\cdot}2, 0{\cdot}5,$ and $1{\cdot}5$. The curves are almost undistinguishable, particularly for $t = 0{\cdot}1$ and $t = 0{\cdot}2$ (remember that $t_1 \simeq 0{\cdot}4039$). Note that the solutions for U plotted in (b) are only valid in the region between the fronts, since there is no water outside it and $U = 0$. However, constant values of U have been plotted outside the water regions to better mark the velocity at the water fronts.

Note that the left water front remains at rest during the complete time interval plotted in that figure. To check the validity of the analytical solution during the initial stages, and the characteristic solution, we have included in Figure 5 the solutions obtained from an alternative finite-volume method (dashed lines; see [9] for the numerical details; the finite-volume method is mostly based on [10]). It is observed that for $t < t_1 \simeq 0{\cdot}4039$ the numerical solution is indistinguishable from the analytical solution.

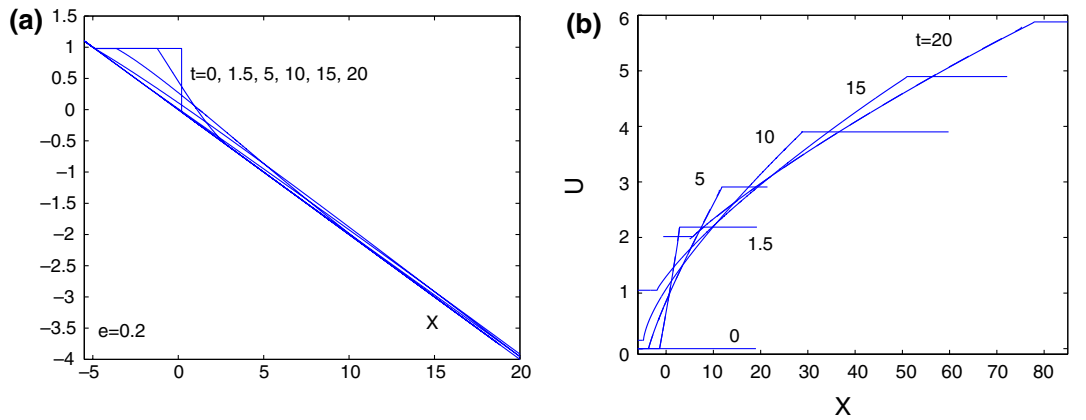

Figure 6. Water depths (a) and velocity U (b) in the original coordinate X along the sloping bed for several instants of time, and for $e = 0{\cdot}2$. Also plotted with dashed lines are the solutions obtained from a finite-volume method [9] at the instants $t = 1{\cdot}5, 5,$ and 20 (they are almost undistinguishable). Note that the solutions for U plotted in (b) are only valid in the region between the fronts, since there is no water outside it and $U = 0$. However, constant values of U have been plotted outside the water regions to better mark the velocity at the water fronts.

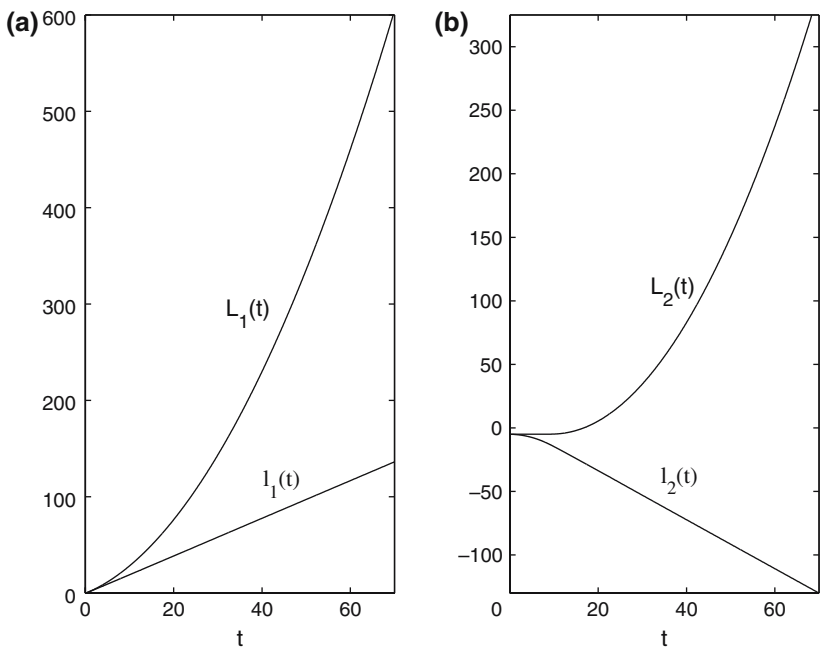

Figure 7. Right (a) and left (b) water fronts in the coordinate x, $l_1(t)$ and $l_2(t)$, and in the coordinate X, $L_1(t)$ and $L_2(t)$. ($t_1 \simeq 0{\cdot}4079, t_2 \simeq 10{\cdot}0985$.)

Figure 6 shows the water depth, and the velocity U, in the original coordinate X up to $t =$ 20 (for larger times, η becomes too small to be appreciated on the scale used in Figure 6(a)). These results were obtained numerically by the method of characteristics (also included with dashed lines are the solutions obtained from a finite-volume method [9]). Figure 7 shows the trajectories of the right and left water fronts in the coordinate x, $l_1(t)$ and $l_2(t)$, and in the coordinate X, $L_1(t)$ and $L_2(t)$. It is observed in Figure 7(b) that the left water front in the X coordinate, $L_2(t)$, remains constant until $t = t_2 \simeq 10{\cdot}0985$, and then moves downward with the rest of the fluid (towards increasing X). In relation to $l_1(t)$ and $l_2(t)$, it is interesting to note

that they become straight lines just after $t > t_1$ and $t > t_2$, respectively [see also Figure 4(a)]. This is a consequence of the fact that the fluid velocity u in the vicinity of the water fronts tend to constant values as time increases. These properties will be used in the next section to generate a similarity solution for large time.

5. Long-time self-similar solution

Figure 8 shows the profiles of c and u for several instants of time up to $t = 70$ for $e = 0{\cdot}2$. Figure 8(a) suggests that the profiles of c tend to become independent of the initial depth distribution as time increases, thus indicating that the problem may have a self-similar solution (of the second kind; see, *e.g.*, [11]) for large t. In addition, Figure 7 shows that the water spreading in the coordinate x is a linear function of time for sufficiently large t. Thus, one may define the self-similar variable

$$\xi \equiv \frac{x - l_2^{\infty}(t)}{l_s^{\infty}(t)}, \quad 0 \le \xi \le 1, \tag{28}$$

with

$$l_s^{\infty}(t) \equiv l_1^{\infty}(t) - l_2^{\infty}(t) = u_m t + l_0, \tag{29}$$

$$l_1^{\infty}(t) = u_1 t + l_{01}, \quad l_2^{\infty}(t) = -u_2 t + l_{02}, \quad u_m = u_1 + u_2, \quad l_0 = l_{01} - l_{02}, \tag{30}$$

where u_1, u_2, u_m, l_0, l_{01} and l_{02} are constants. A first approximation of the solution for large t may be written as

$$c(t, x) = c_m(t) f(\xi), \quad u(t, x) = u_m g(\xi), \tag{31}$$

with

$$f(0) = f(1) = 0, \quad g(0) = -u_2/u_m, \quad g(1) = u_1/u_m. \tag{32}$$

Here $c_m(t)$ is the maximum of c as a function of time for large t, whose functional form may be obtained from the integral form of the mass-conservation equation. Thus, multiplying (7) by c and integrating between $l_1(t)$ and $l_2(t)$, one obtains

$$\int_{l_1(t)}^{l_2(t)} \frac{\partial c^2}{\partial t} \mathrm{d}x + c^2 u \Big|_{l_1}^{l_2} = 0. \tag{33}$$

Since $c = 0$ at $x = l_1$ and $x = l_2$, after applying Leibnitz's rule,

$$\frac{\mathrm{d}}{\mathrm{d}t} \int_{l_1(t)}^{l_2(t)} c^2 \mathrm{d}x = 0, \tag{34}$$

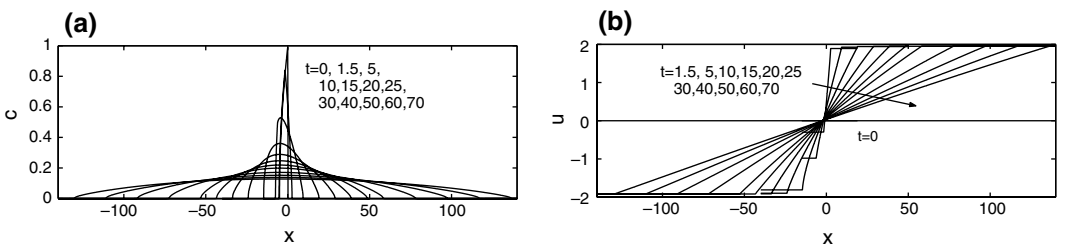

Figure 8. x-profiles of c (a) and u (b) for several instants of time, as indicated, for $e = 0{\cdot}2$.

so that the quantity

$$I \equiv \int_{l_1(t)}^{l_2(t)} c^2 \mathrm{d}x, \tag{35}$$

remains constant in time. From the initial distribution (10), one has

$$I = \frac{1}{2\sin\theta}. \tag{36}$$

The substitution of (31) and (28) in (35) yields

$$I = c_m^2(t) l_s^{\infty}(t) \int_0^1 f^2(\xi)\mathrm{d}\xi. \tag{37}$$

Therefore,

$$c_m(t) = \frac{K_0}{\sqrt{u_m t + l_0}}, \tag{38}$$

where K_0 is a constant that satisfies

$$I = \frac{1}{2\sin\theta} = K_0^2 \int_0^1 f^2(\xi)\mathrm{d}\xi. \tag{39}$$

The substitution of (31), (28) and (38) in the momentum equation (8) gives

$$(u_2 - u_m\xi)g' + u_m g g' + 2\frac{K_0^2}{u_m(u_m t + l_0)} f f' = 0, \tag{40}$$

where primes denote derivatives with respect to ξ. For large t, the last term is small. Hence, as a first approximation, discarding the trivial solution $g' = 0$, one has the linear solution

$$g(\xi) = \frac{u_m\xi - u_2}{u_m}. \tag{41}$$

This solution satisfies both boundary conditions for u [see (28–32)]: for $\xi = 0$ [corresponding to $x = l_2^{\infty}(t)$], $u = -u_2$, and for $\xi = 1$ [$x = l_1^{\infty}(t)$], $u = u_1$. On the other hand, (31) with (38) and (41) satisfy identically the continuity equation (7). Thus, any function $f(\xi)$ in (31) satisfying the boundary conditions $f(0) = f(1) = 0$ is a solution to the problem in the first approximation (31) for large t.

To obtain $f(\xi)$, one has to consider the next approximation to $u(t, x)$ for large t. Writing

$$u(t, x) = u_m[1 + \phi(t)]g(\xi), \tag{42}$$

with g given by (41) and $|\phi| \ll 1$ for $t \gg 1$, and substituting in Equation (8), one obtains

$$(u_m\xi - u_2)\left(\frac{\mathrm{d}\phi}{\mathrm{d}t} + \phi\right) + \frac{2K_0^2}{u_m t + l_0} f f' = 0. \tag{43}$$

This equation has a solution provided that

$$\frac{\mathrm{d}\phi}{\mathrm{d}t} + \phi = \frac{\alpha}{u_m t + l_0} \quad \text{and} \quad f f' = -\frac{\alpha}{2K_0^2}(u_m\xi - u_2), \tag{44}$$

where α is an arbitrary constant. The solution of the first equation is

$$\phi = k_1 \mathrm{e}^{-t} - \frac{\alpha}{u_m}\mathrm{e}^{-t - l_0/u_m} E_1(-t - l_0/u_m), \tag{45}$$

where k_1 is an integration constant and E_1 is the exponential integral function (*e.g.* [12, Chapter 5]). For large t, as a first approximation one has

$$\phi(t) \sim \frac{\alpha}{u_m t + l_0}. \tag{46}$$

The solution of the second equation in (44) can be written as

$$f = \sqrt{k_2 - \frac{\alpha}{2u_m K_0^2}(u_m \xi - u_2)^2}, \tag{47}$$

where k_2 is an integration constant. The boundary condition $f(\xi = 0) = 0$ implies that $k_2 = \alpha u_2^2/(2u_m K_0^2)$. Then, the second boundary condition $f(\xi = 1) = 0$ can only be satisfied if

$$u_1 = u_2 = u_m/2. \tag{48}$$

Thus,

$$f(\xi) = \sqrt{\frac{\alpha u_m}{2K_0^2}(\xi - \xi^2)}. \tag{49}$$

One can obtain the constant α in terms of K_0 by normalizing this function at its maximum value at $\xi = 1/2$, *i.e.*, $f(\xi = 1/2) = 1$, which yields

$$\alpha = \frac{8K_0^2}{u_m}, \quad f(\xi) = \sqrt{4(\xi - \xi^2)}. \tag{50}$$

Finally, K_0 is obtained from (39):

$$K_0 = \frac{1}{2}\sqrt{\frac{3}{\sin\theta}}. \tag{51}$$

Summing up, the self-similar solution for large t can be written as

$$c(t, x) = c_m(t)\sqrt{4(\xi - \xi^2)}, \quad c_m(t) = \frac{1}{2}\sqrt{\frac{3}{\sin\theta}}\frac{1}{\sqrt{u_m t + l_0}}, \tag{52}$$

$$u(t, x) = u_m\,[1 + \phi(t)]\left(\xi - \frac{1}{2}\right), \quad \phi(t) = \frac{6}{u_m \sin\theta (u_m t + l_0)}, \tag{53}$$

with

$$\xi = \frac{x + u_m t/2 - l_{02}}{u_m t + l_0}, \quad 0 \le \xi \le 1. \tag{54}$$

The constants u_m, l_0, and l_{02} (or u_m, l_{01}, and l_{02}) depend on the initial conditions (*i.e.*, just on the slope of the bed e in this problem) and have to be obtained numerically. This is typical of self-similar solutions of the second kind, where some constants have to be obtained by connecting numerically the particular initial condition with the final self-similar state (see, *e.g.*, [11, Section 12.3]).

Numerical solution for the trajectories of the water fronts $l_1(t)$ and $l_2(t)$ for $e = 0{\cdot}2$ (see Figure 7) up to $t = 200$ shows that $l_1 \simeq 1{\cdot}929t + 1{\cdot}81$ and $l_2 \simeq -1{\cdot}929t + 5{\cdot}191$ (note that the numerical values of u_1 and u_2 coincide, as predicted by the self-similar solution). Thus, $u_m \simeq 3{\cdot}858$, $l_0 \simeq -3{\cdot}381$ and $l_{02} \simeq 5{\cdot}191$ for the slope $e = 0{\cdot}2$. Figure 9 shows the solutions, using these numerical values, for $c(t, x)/c_m(t)$ and $u/[u_m(1 + \phi(t))]$ as functions of ξ for several values of t, and compares them with $f(\xi) = \sqrt{4(\xi - \xi^2)}$ and $g(\xi) = \xi - 1/2$, respectively. It is

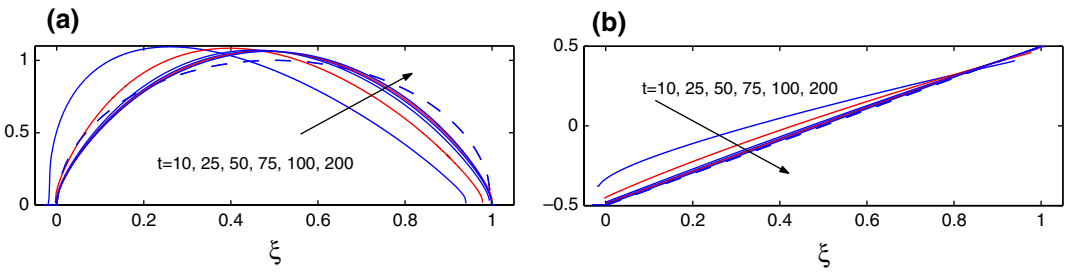

Figure 9. (a): $c(t,x)/c_m(t)$ as a function of ξ for several values of t, as indicated, for $e=0{\cdot}2$; the dashed line corresponds to $f(\xi)=\sqrt{4(\xi-\xi^2)}$. (b): $u(t,x)/[u_m(1+\phi(t))]$ as a function of ξ for several values of t, as indicated, for $e=0{\cdot}2$; the dashed line corresponds to $g(\xi)=\xi-1/2$.

observed that u converges faster than c to the self-similar solution [according to (52–53), u converges to the self-similar solution as t^{-1}, while c converges as $t^{-1/2}$].

In the original variables along the sloping bed, the similarity solution (52–54) reads

$$\eta(t,X)=\frac{3(\xi-\xi^2)}{\sin\theta\cos\theta(u_m t+l_0)}, \tag{55}$$

$$U(t,X)=\sin\theta t+u_m[1+\phi(t)]\left(\xi-\frac{1}{2}\right), \tag{56}$$

$$\xi=\frac{X+(u_m t-\sin\theta t^2)/2-l_{02}}{u_m t+l_0}, \tag{57}$$

with $\phi(t)$ given in (53). This solution is valid for $0\le\xi\le1$; *i.e.*, for

$$L_2^{\infty}(t)\equiv\frac{1}{2}\sin\theta t^2-\frac{u_m}{2}t+l_{02}\le X\le L_1^{\infty}(t)\equiv\frac{1}{2}\sin\theta t^2+\frac{u_m}{2}t+l_0+l_{02}. \tag{58}$$

6. Conclusions

In this paper we have presented analytical solutions of the shallow-water equations valid for different stages of the dam-break flow problem on a constant-slope bed. The different solutions are connected to each other numerically by the method of characteristics. Quantitative results are given for a slope $e=0{\cdot}2$. The model equations are approximately valid for any slope of the bed provided that the characteristic flow length along the bed is much larger than the characteristic length normal to the bed. As discussed in Section 3, the analytical solutions given here are fundamentally different from the classical self-similar solution to the dam-break problem on a horizontal plane due to the finite mass of water released after the rupture of the dam.

One of the main limitations of the given solutions is that friction is neglected, so that caution must be taken when applying these results. However, these frictionless models may capture some of the essential features of the dynamics of the water spreading after the breaking of a dam on an inclined bed, in addition to providing benchmark solutions to validate numerical studies based on the shallow-water equations for the flow upon non-horizontal beds.

In connection with this, we have used both the analytical solution for the spreading of the water front at the initial stages and the similarity solution for large time to validate a finite-volume numerical code for the general flow on an inclined bed of arbitrary slope [9]. The similarity solution may also be used to estimate in a simple way a maximum limit for the velocity of avalanches down a river following a sudden release of water from a ruptured dam. Finally,

this similarity solution may also serve as a simple basic flow to analyze the stability properties of the flow down a sloping channel (when friction is neglected).

Acknowledgements

This research has been supported by the Consejería de Obras Públicas of the Junta de Andalucía (Spain; Ref. 807/31.2116). I thank Patricio Bohorquez for the numerical solutions obtained from a finite-volume method that appear in Figures 5 and 6.

References

1. A. Ritter, Die Fortpflanzung der Wasserwellen. *Z. Verein. Deutsch. Ing.* 36 (1892) 947–954.
2. J.J. Stoker, *Water Waves*. New York: Interscience (1957) 567 pp.
3. B. Hunt, Asymptotic solution for dam break on a sloping channel. *J. Hydraul. Engng.* 109 (1983) 1698–1706.
4. B. Hunt, An inviscid dam-break solution. *J. Hydraul. Res.* 25 (1987) 313–327.
5. J.B. Keller, Shallow-water theory for arbitrary slopes of the bottom. *J. Fluid Mech.* 489 (2003) 345–348.
6. S.B. Savage and K. Hutter, The dynamics of avalanches of granular materials from initiation to run-out. *Acta Mech.* 86 (1991) 201–223.
7. F. Bouchut, A. Mangeney-Castelnau, B. Perthame and J.P. Vilotte, A new model of Saint Venant and Savage-Hutter type for gravity driven shallow water flows. *C. R. Acad. Sci. Paris, Ser. I* 336 (2003) 531–536.
8. W.C. Thacker, Some exact solutions to the nonlinear shallow-water wave equations. *J. Fluid Mech.* 107 (1981) 499–508.
9. P. Bohorquez and R. Fernandez-Feria, Transport of suspended sediment under the dam-break flow on an inclined bed of arbitrary slope. *J. Hydraul. Res.* (submitted).
10. J. Burguete and P. Garcia-Navarro, Efficient construction of high-resolution TVD conservative schemes for equations with source terms: application to shallow water flows. *Int. J. Numer. Meth. Fluids* 37 (2001) 209–248.
11. G.I. Barenblatt, *Scaling, Self-similarity, and Intermediate Asymptotics*. Cambridge: Cambridge University Press (1996) 386 pp.
12. M. Abramowitz and I.A. Stegun, *Handbook of Mathematical Functions*. New York: Dover (1965) 1046 pp.